

A theoretical analysis of small Pt particles on rutile $\text{TiO}_2(110)$ surfaces

Veysel Çelik,¹ Hatice Ünal,¹ Ersen Mete,^{1,*} and Şinasi Ellialtıoğlu²

¹Department of Physics, Balıkesir University, Balıkesir 10145, Turkey

²Department of Physics, Middle East Technical University, Ankara 06531, Turkey

(Dated: August 24, 2010)

The adsorption profiles and electronic structures of Pt_n ($n=1-4$) clusters on stoichiometric, reduced and reconstructed rutile $\text{TiO}_2(110)$ surfaces were systematically studied using on site $d-d$ Coulomb interaction corrected hybrid density functional theory calculations. The atomic structure of small Pt cluster adsorbates mainly depend on the stoichiometry of the corresponding titania support. The cluster shapes on the bulk terminated ideal surface look like their gas phase low energy structures. However, for instance, they get significantly distorted on the reduced surfaces with increasing oxygen vacancies. On non-stoichiometric surfaces, Pt-Ti coordination becomes dominant in the determination of the adsorption geometries. The electronic structure of $\text{Pt}_n/\text{TiO}_2(110)$ systems can not be correctly described by pure DFT methods, particularly for non-stoichiometric cases, due to the inappropriate treatment of the correlation for d electrons. We performed DFT+U calculations to give a reasonable description of the reconstructed rutile (110) surface. Pt clusters induce local surface relaxations that influence band edges of titania support, and bring a number of band-gap states depending on the cluster size. Significant band gap narrowing occurs upon Pt_n -surface interaction due to adsorbate driven states on the bulk terminated and reduced surfaces. On the other hand, they give rise to a band gap widening associated to partial reoxidation of the reconstructed surface. No metallization arises even for Pt_4 on rutile.

PACS numbers: 68.43.Bc, 68.43.Fg

I. INTRODUCTION

Transition metal oxides are important because of their wide range of technological applications. Naturally occurring rutile polymorph of titanium dioxide is a generic material because of its abundance, non-toxicity, and stability under atmospheric conditions. The (110) termination of rutile TiO_2 is energetically the most stable surface among the other low index facets.¹ For these reasons, rutile $\text{TiO}_2(110)$ structure is a prototypical material to understand the catalysis on more complex oxide surfaces.^{2,3} Its reducibility (either by oxygen vacancy formation or alkali metal adsorption) raises a great interest for fundamental study of photo- and heterogeneous catalysis⁴⁻⁶, functional ultrathin films^{7,8}, and dielectrics.^{9,10} These applications rely mainly on the surface electronic properties of titania.

In TiO_2 bulk structure, Ti atoms are sixfold and oxygens are threefold coordinated. Rutile (110) surface has these types of atoms, such as basal atoms B1 and Ti6c, which exhibit bulk like bonding characteristics as depicted in Fig. 1. The (110) termination of the bulk lattice breaks the Ti-O bonds which lie normal to the surface plane resulting in fivefold Ti and twofold O atoms on the surface. Those are denoted as Ti5c and O1 in Fig. 1, respectively. The undercoordinated bridging oxygens, O1, are exposed on the surface. They form oxygen rows along [001] direction. The atomic disposition of this stoichiometric long range ordered (1×1) phase has been well established by experimental methods^{3,11-17} and by *ab initio* calculations.¹⁸⁻³⁵

By means of ion bombardment or thermal annealing, the surface can be reduced through oxygen removal.

Its oxygen vacancy induced reducibility enhances hetero- and photocatalytic activity by giving rise to rich surface chemistry. In this sense, rutile (110) system becomes an excellent model substrate that shows interesting properties of more complex metal oxides.³⁶⁻⁴⁰

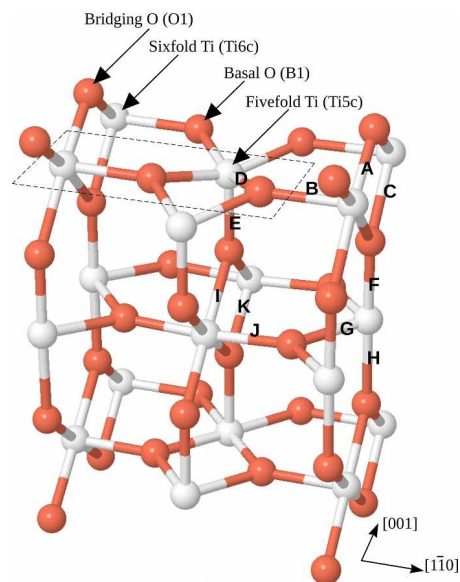


FIG. 1. (color online) Optimized atomic structure of bulk terminated rutile $\text{TiO}_2(110)$ surface. Actual computational cell has 15 atomic layers also referred as 5 trilayers. The model shows only 3 out of 5 trilayers. Black (red) and white balls represent O and Ti atoms, respectively. Dashed rectangular area denotes the (1×1) surface unit cell. The bond labels are indicated as capital letters that run from A to K.

Although DFT is successful in describing ground state atomic and electronic structure of many semiconductors, there is still a debate on the choice of method, pure or hybrid, employed within the framework of DFT to improve the accuracy to estimate the material properties. Particularly, some of DFT predicted properties of reconstructed and reduced TiO_2 surfaces are inconsistent with the experimental data.^{41,42} This is due to inadequate description of strongly correlated $3d$ electrons of Ti atoms.^{43–45}

Since bulk termination gives rise to a sharp discontinuity in the atomic bonds, rutile (110) is known occasionally to undergo surface morphological reconstructions.^{46–55} This phase transition is believed to be assisted by annealing that reduces the surface and leads to a (1×2) reconstruction. The three dimensional determination of such atomic rearrangements on reconstructed rutile (110) surface is difficult by experimental techniques.⁵⁵ Onishi and Iwasawa proposed the Ti_2O_3 added row model for the reconstructed rutile (110) surface.⁴⁶ There are also some controversial experimental results. For example, Park *et al.*⁵⁴ suggested a new model where Ti are on interstitial sites forming a relatively more O deficient surface stoichiometry. This model recently confirmed experimentally by Shibata *et al.*⁵⁵ Although it is a matter of debate, the added row model of Onishi and Iwasawa remains to be widely assigned (1×2) rutile (110) reconstruction.^{47–50,52}

The steps and point defects such as oxygen vacancies and (sub)surface impurities shown in scanning tunneling microscopy (STM) images play an important role in electronic properties of TiO_2 surfaces⁴⁰. Understanding of the fundamental aspects of defects and impurities on titania surfaces are important for technological applications. In addition, the catalytic activity of TiO_2 surfaces can be promoted by transition metal (such as Au or Pt) doping⁵⁶ or adsorption^{57,58}. Therefore, the interaction of surface defects with functional adsorbates is crucial for both fundamental research and practical applications. For example, Pillay and Hwang⁵⁹ studied the adsorption geometries of small Au, Ag, and Cu clusters on rutile (110) surface. Recently, Gong *et al.*⁶⁰ investigated the atomic structures of small Au and Pt clusters supported on defect and regular sites of anatase $\text{TiO}_2(101)$ surface.

In this work, our primary aim is to study the adsorption sites, geometries and resulting electronic structures of Pt_n ($n=1-4$) clusters on the stoichiometric, reduced (by bridging oxygen B1 removal) and reconstructed (added row model⁴⁶) rutile $\text{TiO}_2(110)$ surfaces using *ab initio* calculations. In order to gain insight into the growth pattern of small Pt particles on these surfaces, we chose a single Pt adsorbate as the starting point. Then, we studied the adsorption profiles of Pt_n by adding extra Pt atoms at different probable adsorption sites to the previously optimized Pt/ $\text{TiO}_2(110)$ system. Alternatively, we also put Pt particles, whose geometries were optimized in their gas phase, on probable adsorption sites. By comparing these two distinct approaches we decided on the lowest energy adsorption structures of small Pt particles on the surfaces considered.

II. COMPUTATIONAL DETAILS

Total energy density functional theory (DFT) calculations were carried out using the Vienna *ab-initio* simulation package (VASP).⁶¹ Nonlocal exchange–correlation energies were treated with Perdew–Burke–Ernzerhof (PBE)⁶² functional based on the generalized gradient approximation (GGA). We used projector-augmented waves (PAW) method^{63,64} to describe the ionic cores and valence electrons with an energy cutoff value of 400 eV for the plane wave expansion.

Pure DFT methods systematically fail in describing strongly correlated $3d$ electrons localized on Ti atoms, particularly in the case of reduced rutile (110) surface.^{43–45} This comes from the inherent shortcoming of the DFT due to the lack of proper self-energy cancellation between the Hartree and exchange terms as in Hartree–Fock theory. DFT+U approach is an alternative attempt to compensate this localization deficiency by introducing additional Hubbard U term for electron on-site repulsion. Therefore, in order to get a sound description of Pt_n adsorption on reduced and reconstructed $\text{TiO}_2(110)$ surfaces, we performed Hubbard U corrected DFT calculations using Dudarev’s approach.⁶⁵ We supplemented PBE exchange–correlation functional with Dudarev $U-J$ term acting on Ti $3d$ states, that we refer as GGA+U. This empirical term is adjusted to give reasonable agreement with the experimental data. Morgan and Watson fitted the U parameter to 4.2 eV in order to reproduce the experimentally observed position of oxygen vacancy driven Ti defect state in the band gap.⁴³ In the same manner, our tests suggested to choose the parameters $U=4.5$ eV and $J=0$ eV to obtain a reasonable electronic description of the added row model of Onishi and Iwasawa as well as the gap state at the reduced surface.

Theoretical studies employing other hybrid methods such as incorporation of the exact Fock exchange energy (EXX) with various percentages, recently, revisited the stoichiometric rutile $\text{TiO}_2(110)$ surface.³⁰ Zhang *et al.* reproduced many of the experimental bulk and stoichiometric surface properties of TiO_2 by adjusting the mixing of HF exchange contribution. Further investigations are still needed to see if EXX approach can correctly describe the defect states.

Computationally, there has been another debate about the slab thickness to correctly predict the surface energetics as well as the atomic structure. The surface energy is known to fluctuate with slab thickness.^{9,19,28,31–34} For adsorption of small molecules on the bulk terminated surface, Thompson *et al.*³² suggested 4 layers of O– Ti_2O_2 –O units (also referred as trilayers) with the two bottom layers fixed to their bulk positions. Kowalski *et al.*³⁴ additionally suggested the saturation of the dangling bonds at the bottom surface with pseudohydrogens having nuclear charges of $+4/3$ and $+2/3$, correspondingly.

Our stoichiometric slab model consists of 15 atomic layers that correspond to 5 layers of O– Ti_2O_2 –O units. This model has a mirror symmetry with respect to the

central atomic plane. The dashed rectangular region shown in Fig. 1, represents $p(1\times 1)$ periodicity. The corresponding surface unit cell is composed of a central Ti_2O_2 planar arrangement with two oxygens symmetrically cross bonded to the nearest neighbor in-plane Ti atom from above and from below. These units are shifted by half its length along $[\bar{1}10]$ between adjacent layers as seen in Fig. 1 which shows three out of the five layers in our model. The slab was separated from its images along the surface normal by a vacuum region of ~ 14 Å.

For geometry optimizations, the Brillouin zone integrations were carried out with $2\times 2\times 1$ Monkhorst-Pack⁶⁶ k -point grid for unreconstructed (bulk terminated and reduced) and reconstructed cells with surface periodicities $p(4\times 2)$ and $p(4\times 1)$, respectively. The spin polarization was found to be negligibly small for the Pt_n on stoichiometric surface considered in this work. This is in agreement with the similar findings of Iddir *et al.* for single Pt adsorbate on $\text{TiO}_2(110)$ ⁵⁸. We performed spin polarized GGA+U calculations for Pt_n/TiO_2 systems where magnetization is non-negligible, in particular, for reduced and reconstructed surface cases. A full geometry optimization was fulfilled with residual minimization method direct inversion in the iterative subspace (RMM-DIIS) scheme preconditioned by a few non-selfconsistent Davidson-block iterations as implemented in the code. We required a precision of 10^{-2} eV/Å in the residual forces in every spatial component on all the atoms without fixing them to their bulk positions.

We estimated the binding energies of Pt clusters by,

$$E_{\text{Pt}_n}^{\text{b}} = E_{\text{Pt}_n/\text{TiO}_2} - E_{\text{TiO}_2} - E_{\text{Pt}_n},$$

where $E_{\text{Pt}_n/\text{TiO}_2}$, E_{TiO_2} and E_{Pt_n} are the total energies of the Pt_n/TiO_2 combined system, the bare TiO_2 slab and the corresponding Pt_n cluster, respectively. The average adsorption energy per atom, $E_{\text{Pt}_n}^{\text{c}}$, can be calculated by dividing $E_{\text{Pt}_n}^{\text{b}}$ by the cluster size n .

III. RESULTS & DISCUSSION

We made extensive tests for the choice of the slab model by changing the slab thickness, the number of fixed atomic layers within, and the size of the vacuum spacing, provided that the (110) facet possesses 4×2 cell symmetry to avoid any interaction between the periodic images of Pt cluster adsorbates. The results suggest that no atom, particularly near the surface, should be fixed to its bulk position in order to avoid stress driven gap states and that the slab model has to be at least 5 trilayers thick (15 atomic layers) to ensure a bulk-like central part. Similarly, for instance, Kiejna *et al.*³¹ found that surface energetics are very sensitive to lattice relaxations by considering the effect of various slab model thicknesses. Other hybrid DFT approaches with different exchange and correlation treatments are known to have a small effect on the surface atomic configurations³⁰.

TABLE I. The comparison of computational and experimental bond lengths for the bulk terminated stoichiometric $\text{TiO}_2(110)$ surface. All measurements are in angstroms. Bond labeling follows similar to those of Thompson *et al.* as shown in Fig. 1.

Bond	Experimental		Theoretical			
	Ref. ¹⁵	Ref. ¹⁷	Ref. ²⁵	Ref. ^{32a}	GGA ^b	GGA+U ^b
A	1.71±0.07	1.85	1.80	1.84	1.85	1.88
B	2.15±0.09	2.15	2.04	2.04	2.03	2.03
C	1.99±0.09	2.08	2.09	2.11	2.10	2.09
D	1.84±0.05	1.90	1.95	1.92	1.95	1.95
E	1.84±0.13	1.79	1.85	1.83	1.84	1.90
F	1.97±0.12	1.90	1.90	1.89	1.90	1.95
G	1.99±0.05	2.00	1.97	1.98	1.98	1.97
H	2.18±0.11	2.11	2.11	2.13	2.12	2.12
I	2.00±0.08	2.01	2.02	2.02	2.02	2.01
J	1.92±0.06	1.92	1.97	1.96	1.96	1.96
K	1.94±0.06	1.89	1.90	1.91	1.92	1.95

^a values for 5 layer slab model

^b results of present calculation with PBE xc functional

Indeed, a comparison of our calculated bond lengths for the stoichiometric rutile $\text{TiO}_2(110)$ surface shows a good agreement with the available experimental^{15,17} and theoretical^{25,32} results as presented in Table I. Moreover, the incorporation of supplemental Coulomb repulsion to correct the correlation energy by inclusion of Dudarev $U = 4.5$ eV term for Ti 3d electrons did not distort the atomic positions, considerably. In addition to these structural properties, we also calculated the binding energies (BE) of Pt to be 2.32 eV and 3.32 eV on the stoichiometric and partially reduced (with oxygen vacancy concentration of $\theta=1/8$) surfaces, respectively. Our values are presented in Table II and are only slightly larger than the previous theoretical results of Iddir *et al.*⁵⁸ This can be well addressed to the difference in slab thicknesses and in surface areas of computation cells. In particular, the oscillatory convergence behavior of the surface electronic properties depending on the number of trilayers, included in a slab calculation, was also confirmed by other studies.^{31,32,34,35} From computational point of view, a slab with large number of trilayers is expected to give very well converged results for Pt clusters on 4×2 cell. However, independent of slab thickness, the electronic description of defect states such as the oxygen vacancies is problematic with pure DFT methods.^{43–45} In the same line, our tests showed that standard DFT fails in describing the electronic structure of the added row model of reconstructed surface, as well, by giving surface Ti 3d state in the conduction band (CB). This study, particularly, focuses on a reasonable electronic description of small Pt clusters on rutile (110) surface where spin polarization is non-negligible. Therefore, our GGA+U values for this slab model would not only give very well con-

verged bond lengths, as presented in Table I, but also yield the energetics reasonably accurate for a Pt cluster adsorption system on specifically non-stoichiometric rutile (110) surfaces.

In order to study the adsorption characteristics of Pt_n ($n = 1-4$) particles on rutile $\text{TiO}_2(110)$ surfaces we first considered these in the gas phase and performed non-collinear spin polarized DFT calculations. A recent work stresses the necessity for inclusion of spin-orbit interactions in a relevant calculation to understand the physics of Pt clusters⁶⁷. However, the ground state geometries being a dimer for Pt_2 , a triangle for Pt_3 and a bent (off-planar) rhombus in the case of Pt_4 seem to be less affected by spin-orbit coupling.

For Pt dimer, our non-spin-orbit calculations resulted in triplet electronic ground state with a binding energy (BE) of 1.819 eV/atom and gave the bond length to be 2.331 Å. The calculated dimer length shows an excellent agreement with the experimental value of 2.333 Å⁶⁸⁻⁷⁰, while our result for the BE is slightly higher than the experimental value of 1.570 eV/atom. When we included self-consistent noncollinear spin-orbit coupling that resulted in the same magnetic ground state, the BE decreases to 1.665 eV/atom whereas the dimer bond length increases to 2.382 Å. These values are sensitive not only to the inclusion of spin-orbit effects but also to the exchange-correlation scheme employed. For instance, by performing GGA-PW91 calculations, Huda *et al.*⁶⁷ determined different spin multiplicities for the ground state of Pt_3 cluster depending on the spin-orbit coupling. However, our GGA-PBE calculations gave singlet ground states for Pt_3 having average binding energies of 2.184 and 2.376 eV/atom with and without LS coupling, respectively. Moreover, Huda *et al.* reported that spin-orbit interaction drives the geometry from an equilateral to an isosceles triangle. Pt_3 with GGA-PBE, on the other hand, develops equilateral coordination with bond lengths of 2.49 Å while the inclusion of spin-orbit interaction extends all bonds slightly and equally to 2.50 Å. Our GGA-PBE binding energy value agrees well with a previous theoretical result.⁷¹ In addition, incorporation of spin-orbit coupling leads to an excellent agreement with an old experimental estimate of 2.18 eV/atom.⁷²

Pt_4 has a quintet electronic ground state (GS) with GGA-PBE, leading to an off-planar rhombus geometry that has a side bond length of 2.51 Å and a bending angle of 23.3°. We calculated atomic BEs to be 2.515 eV/atom with, and 2.686 eV/atom without the LS coupling. These values are comparable with the previous results.^{67,73} However, spin-orbit interaction included in the GGA-PBE calculation did not make the geometry perfectly planar as reported for GGA-PW91.⁶⁷ It slightly extends the bond lengths to 2.52 Å by decreasing the bending angle to 13.1° and gives the same spin multiplicity for the GS. Consequently, for all isolated small Pt particles considered in this study, inclusion of LS coupling in GGA-PBE exchange-correlation scheme does not deform the GS cluster shapes into new geometries.

A. Pt_n on stoichiometric rutile $\text{TiO}_2(110)$ surface

Pure DFT with GGA-PBE functional gives a band gap of 1.48 eV for the stoichiometric rutile $\text{TiO}_2(110)$ surface. Supplemental Hubbard U on-site repulsion, acting on the Ti 3d electrons, heals this band gap to 2.01 eV by correcting the underestimation in the correlation energy. Although the Dudarev U parameter can be adjusted to a larger value to get a better agreement with the experimental value of ~ 3 eV¹, this would significantly distort the atomic structure. Therefore, without losing the consistency of calculated atomic positions and bond lengths with the experimental values (as presented in Table I), we set it to $U = 4.5$, in consistency with the previous theoretical studies⁴³⁻⁴⁵, to get the Ti defect state in the band gap of the reduced surface and to obtain a reasonable electronic description of the added row model of the reconstructed surface. In both reduced and reconstructed cases, pure DFT methods incorrectly pin the defect states inside and to the lower part of the conduction band (CB) which indicates a tendency for strong delocalization.

GGA+ U calculations were performed using 4×2 cell in order to avoid any charge transfer between the periodic images of Pt clusters on the bulk terminated (110) surface. Moreover, in order to obtain the energetics correctly, we first investigated the magnitude of spin-polarization for small Pt clusters on the surface. The results gave negligibly small spin multiplicities for the ground states of $\text{TiO}_2(110)$ supported Pt_n clusters and for the bare surface, as well. In particular, similar findings were reported by Iddir *et al.* for Pt/ $\text{TiO}_2(110)$ system.⁵⁸ Therefore, adsorption profiles [Fig. 2] and electronic structures [Fig. 3] were calculated without spin polarization for the case of stoichiometric surface.

Relaxed atomic positions for defect free surface are presented in Table I. Our GGA and GGA+ U values do not considerably differ from each other and are in good agreement with previous theoretical calculations^{22,25,29,31-33} as well as the experimental results.^{15,17} The only discrepancy, which exists for all DFT studies, is seen in Ti6c-B1 bond (B in Fig. 1). In order to inspect its relevance to the number of layers, we also performed relaxation calculations with 7 and 8 trilayer cells, that reproduced the same value. Therefore, it can be well addressed to GGA-PBE exchange-correlation functional that underestimates Ti6c-B1 in-plane bond length by 0.12 Å. In addition, experiments reported slightly different results for bond length between Ti6c and the nearest neighbor subsurface oxygen (C in Fig. 1). For this particular bond distance, our GGA and GGA+ U values are consistent with the result of Charlton *et al.*¹⁵ more than the recent result of Lindsay *et al.*¹⁷ Agreement with the experimental data gets better for deeper subsurface bond lengths.

The density of states (DOS) structure for the bare surface is presented in the first panel of Fig.3. The Fermi energy is set to be the zero of energy scale and located just above the valence band maximum (VBM). The upper part of the VB shows dominant O 2p character with a

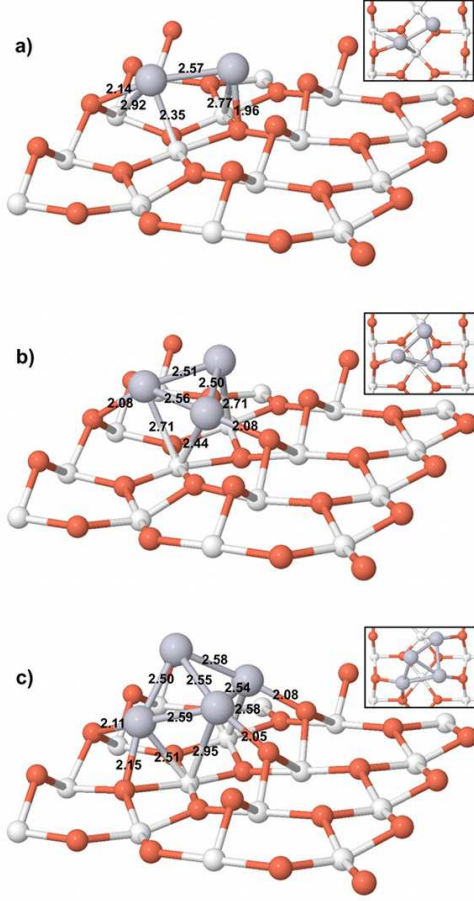


FIG. 2. (color online) Minimum energy structures of Pt_n ($n=2-4$) adsorbed on stoichiometric rutile $TiO_2(110)$ surface. O, Ti, and Pt atoms are denoted by black (red), white small balls and gray big balls, respectively. Pt dimer, trimer, and tetramer on this surface are depicted in (a), (b), and (c), respectively. Measurements are shown, on the corresponding bonds, all in angstroms. The top view of the small Pt particles are presented in the insets to provide better description of the adsorption sites.

non-negligible Ti 3d contribution. Top of the VB mainly composed of O1 states giving a peak ~ 0.4 eV below the VBM. The contribution from the basal oxygens, B1, lies relatively lower in energy inside the VB. Our site projected DOS analysis for the VB agrees well with previous studies, (e.g. hybrid PBE0 result of Labat *et al.*³⁵ and pure GGA result of Sano *et al.*²⁹). The lower part of the conduction band (CB) is dominated by Ti 3d states. The bottom of CB shows a hybrid Ti5c-B1 character with a large Ti contribution. Although, the composition of the CB have some similarities, we have considerable disagreement in the shape of the CB edge with other GGA and PBE0 results^{29,35}. This is due to on-site U repulsion acting on the Ti 3d electrons that causes charge localization

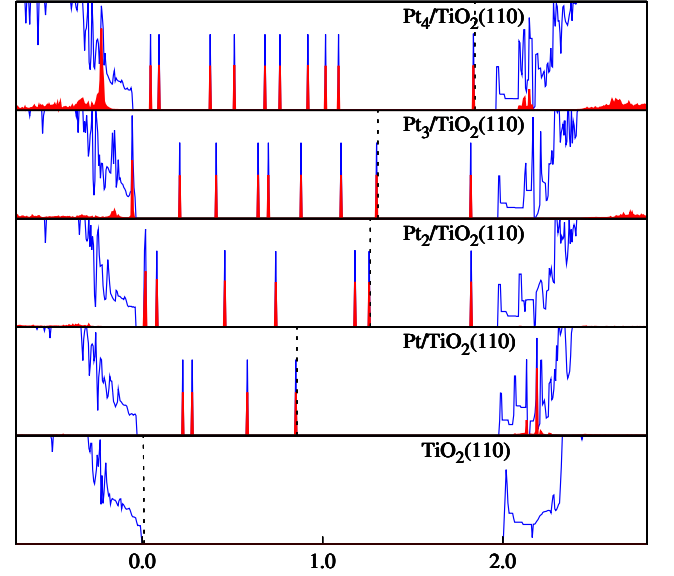


FIG. 3. (color online) Calculated projected and total density of states (DOS) structures for Pt_n ($n=1-4$) on stoichiometric rutile $TiO_2(110)-4 \times 2$ surface. Upper three panels correspond to the atomic structures presented in Fig. 2.

around the atomic Wigner-Seitz radii. Dudarev's U supplements correlation energy of d electrons that elevates the corresponding band offsets to higher energies giving a gap of 2.01 eV. Moreover, it induces differences in the dispersion of Ti 3d states, particularly, near the conduction band minimum (CBM).

Binding of a single Pt atom to the stoichiometric surface was investigated for all possible adsorption sites. We found the lowest energy position of Pt at the hollow site over the Ti5c, leaned toward the nearest bridging oxygen, O1. This adsorption position was also reported previously by GGA-PBE calculations⁵⁸. The calculated BE is 2.32 eV at the hollow site where Pt-O and Pt-Ti bond lengths become 1.96 and 2.49 Å, respectively. Pt atom pulls Ti5c slightly up out of the surface plane by 0.15 Å, and also draws O1 off the bridging oxygen row so that the bond length between this oxygen and Ti6c extends to 2.04 Å from its bare surface value of 1.88 Å [in Table I]. These values are slightly larger than the GGA-PBE results due to additional on-site Coulomb repulsion between Ti 3d electrons with Dudarev $U = 4.5$ eV. For instance, O1-Ti6c bond length increases by 0.03 Å from its GGA-PBE value of 1.85 Å.

The DOS for Pt/TiO₂(110) presented in Fig. 3 indicates that single Pt at the hollow site interacts with Ti5c that appears as a Pt-Ti5c hybridization peak at the bottom of the CB. The non-bonding excess charge around Pt brings four occupied flat gap states within a range of 0.9 eV above the VBM. In addition to the band gap narrowing, these impurity states increases visible range transition probability upon a vertical excitation. This will lead to a metal-to-substrate charge transfer, useful

for solar cell applications.

Energetically preferential adsorption geometry of Pt dimer is shown in Fig. 2a. This atomic structure happens when a second Pt is attached to the Pt/TiO₂ system as to form a dimer. While one of the Pt atoms is already at the hollow site the other one finds its minimum energy position above basal oxygen, B1. It also weakly pulls the nearest neighbor O1 slightly distorting it out of the oxygen row at a separation of 2.39 Å. Alternatively, we placed Pt dimer as a whole on the surface at possible adsorption sites and found the same geometry between the oxygen rows as the minimum energy structure. Pt–Pt bond distance becomes 2.57 Å that is meaningfully larger than the isolated Pt dimer length by 0.24 Å.

Adsorption of Pt trimer breaks its gas phase equilateral symmetry and causes local deformations at the surface plane and in the second subsurface layer as seen in Fig 2b. This geometry is obtained through Pt₂/TiO₂ system by an additional Pt atom as to form a triangular clustering so that it coordinates with the nearest neighbor O1 at the second oxygen row. Pt₃ at different adsorption sites is energetically not preferable. The two Ti5c under the cluster are lifted up by ~ 0.23 Å and B1 atoms, coordinated to these Ti5c, are pushed down by 0.5 Å from their relaxed clean surface positions. The longest Pt–Pt bond length occurs as a result of the pulling of the bridging oxygens from the two sides so that it slightly stretches from 2.50 Å to 2.56 Å. Meanwhile, the shortest Pt–Pt bond is 2.46 Å between the Pt's at the hollow and the Ti5c sites.

Electronically Pt₂ and Pt₃ on the stoichiometric surface yield very similar DOS structures except the number and the band energies of cluster-driven impurity states below the Fermi energy. Pt dimer brings six occupied states within the range of 1.30 eV above the VB and an empty flat going gap state 0.15 eV below the CB. Therefore, Pt₂ on the surface causes a band gap narrowing of 1.45 eV with respect to that of the clean surface. The interaction between the additional Pt at Pt₃ and the substrate occurs essentially with the nearest neighbor O1 on the second oxygen row in Fig. 2b. It brings two more occupied flat states, one of them at the VBM, and causes a shift in band energies of the gap states. In the case of Pt₃, metal driven empty gap state lies almost at the same position with that of Pt₂/TiO₂(110). Resulting band gap narrowing is calculated to be 1.50 eV.

Pt–O1 coordination number increases to three as the cluster size adds up to Pt₄. Although it gives the strongest total binding of 2.98 eV (in Table II), BE per Pt of 0.75 eV proves to be the lowest among the other adsorbates. The reason for this is that one of the Pt atoms lying above the other three makes no contact with the surface. Pt₄ particle on the surface occurs to be slightly distorted bent-rhombus similar to its isolated GS structure (in Fig. 2c). Electronically, Pt₄/TiO₂(110) system features the lowest energy band gap by filling the upper lying flat gap state that is 0.13 eV below the CB. The position of this state is almost the same for the multi-

platinum adsorbates and is empty in the cases of Pt₂ and Pt₃ structures. Altogether, Pt₄ brings a total of ten occupied gap states. It couples to the surface by giving significant contribution to the upper part of the VB essentially by three Pt–O1 hybrid bondings and at the bottom of the CB by three Pt–Ti5c coordinations.

For all cases, adsorption of small Pt particles causes considerable local distortions that are mediated by the neighboring atoms to the second trilayer underneath and are proportional to the cluster size. Although Pt_n adsorbates induce surface deformations, clusters themselves seem to be less affected by forming structures similar to their gas phase low energy geometries on stoichiometric rutile (110) surface. This indicates that the metal–metal coordination within the clusters is stronger than the cluster–substrate interaction.

B. Pt_n on reduced rutile TiO₂(110) surface

Reduced surface is constructed using the relaxed stoichiometric 4×2 cell with 5 trilayers. We removed a single bridging oxygen, O1, from both surfaces to avoid formation of an unreal dipole across the slab. Isolated oxygen vacancies are experimentally observed to produce defect states in the band gap 0.7–0.9 eV below the CB.^{36–39} Pure DFT methods tend to give too delocalized solution where excess charge density occupies the bottom of the CB. Morgan *et al.*⁴³ suggested that a spin polarized GGA calculation, corrected by Hubbard *U* with $U \geq 4.2$ eV reproduces the experimentally observed gap state. Our choice of $U = 4.5$ eV falls within this range and gives the defect state in the gap ~ 1.2 eV below the CB as shown in the lower panel of Fig. 5. Spin multiplicity at the GS happens to be 4 for the 4×2 cell with two reduced surfaces. The position of the defect states is sensitive to atomic relaxations that depends on the choice of the Dudarev *U* parameter. Calzado *et al.*⁴⁴ also showed that gap states move closer to the CB edge as the oxygen vacancy concentration increases in agreement with the UPS observations^{36,74}.

Single Pt atom finds its minimum energy position at the bridging oxygen vacancy site with equal Pt–Ti6c bond lengths of 2.41 Å each. Pt oxidizes the surface such that the vacancy induced topographical deformations recover. The combined system looks like the 4×2 stoichiometric surface cell except that one of the bridging oxygens replaced by a Pt atom which stays 0.7 Å above the oxygen row level. Therefore, Pt adsorption at the defect site gives a strong binding of 3.32 eV compared with that of the stoichiometric case.

We also investigated Pt adsorption on fully reduced rutile(110) surface. At high oxygen vacancy concentrations, an isolated Pt atom takes the place of the nearest neighbor threefold coordinated basal oxygen, B1; an effect also known as the strong metal support interaction (SMSI). Then, B1 loses its coordination with Ti5c and moves to the nearest vacancy site to form a bridge con-

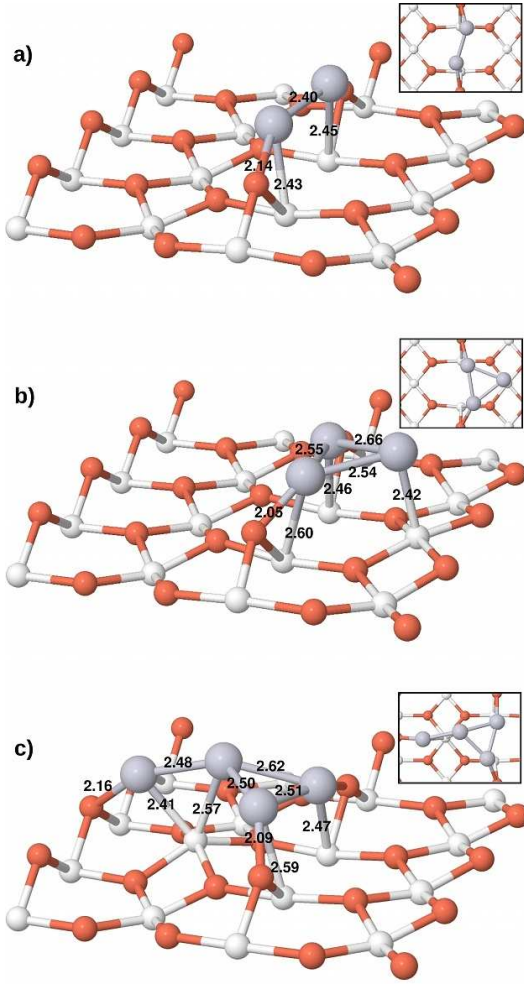


FIG. 4. (color online) Minimum energy structures of Pt_n ($n = 2 - 4$) adsorbed on partially reduced rutile TiO₂(110) surface. O, Ti, and Pt atoms are denoted by black (red), white small balls, and gray big balls, respectively. Pt dimer, trimer, and tetramer on this surface are depicted in (a), (b), and (c), respectively. Measurements are shown, on the corresponding bonds, all in angstroms. The top view of the small Pt particles are presented in the insets are provided for visual convenience.

figuration so that the surface gets oxidized. Pt at B1 site causes considerable local geometric deformations while B1 becomes a twofold coordinated O1.

The site projected DOS structure of the Pt/pr-TiO₂ system is shown in Fig. 5. The contribution of single Pt adsorbate is seen below the Fermi energy indicated as the dark shade (red). The ground state of a Pt atom is d^9s^1 . Therefore, Pt makes two strong bonds with Ti6c at the vacancy site. The BE is 3.32 eV this is 1 eV larger than that on the stoichiometric surface. These bonding energy states fall within the valence band. Pt at the defect site has a significant influence on the local surface reconstruction. This is clearly seen when one compares the DOS structures at the VBM, before and after Pt adsorption on pr-TiO₂. Pt adsorbate also brings four occupied gap

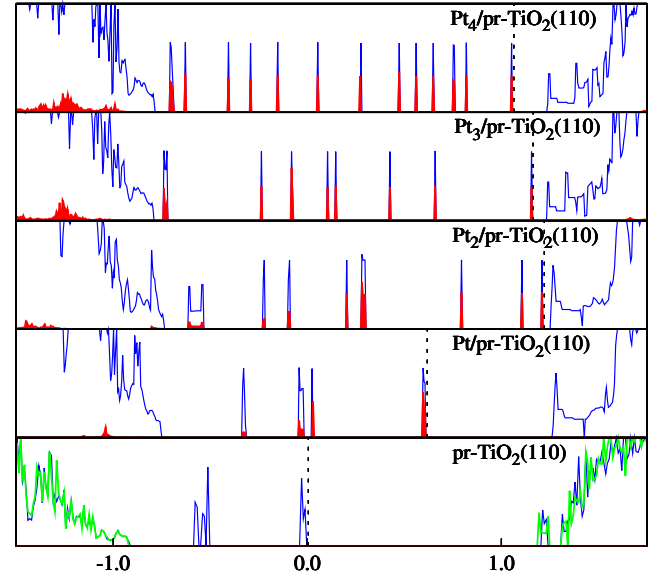


FIG. 5. (color online) Calculated projected and total DOS structures for Pt_n ($n = 1 - 4$) on partially reduced (pr) rutile TiO₂(110)-4×2 surface. Upper three panels correspond to the adsorption geometries in Fig. 4.

states. Upper lying two of them have strong Pt contribution at 0.78 and 1.37 eV above the VBM. Only the third one below the Fermi energy shows a weak dispersion. Others are all flat showing non-bonding character. Lowest lying flat band is 0.43 eV above the VBM.

Adsorption geometries of Pt_n for $n = 2 - 4$ on oxygen defective surface are shown in Fig. 4 where pr-TiO₂(110) stands for partially reduced rutile TiO₂(110) surface associated with oxygen vacancy concentration of 1/8. Pt₂ binds to the reduced surface at the vacancy site as shown in Fig. 4a. Each Pt atom relaxes atop Ti6c site at each side so that the dimer tends to align with the oxygen row. Pt₂ at the defect site pushes Ti6c atoms down from their in plane positions causing considerable distortion on the Ti6c row. Pt-Pt bond length shortens to 2.40 Å from its isolated value of 2.52 Å as a result of strong binding. The BE per Pt atom was calculated to be 1.11 eV that is larger than that of Pt dimer on the stoichiometric surface due to the oxygen vacancy.

We have traced a number of possible adsorption geometries for Pt₃ particle on the defective surface. Pt₃/pr-TiO₂(110) in Fig. 4b represents the minimum energy geometry of the trimer whose initial structure is obtained by adding a Pt atom to the Pt dimer in Fig. 4a. This additional Pt gets adsorbed at Ti5c site and pulls it up by ~ 0.40 Å from its in plane position. Resulting Pt-Ti5c bond length becomes 2.42 Å. Due to imperfect alignment of the Pt dimer along the surface oxygen row this triangular cluster shape becomes slightly distorted compared with the equilateral triangle of gas phase Pt₃.

Pt₂ and Pt₃ adsorbates give very similar DOS characteristics on the reduced surface. For both cases, eight im-

purity states fall within the band gap as shown in Fig. 5. One expects to get narrower band gaps as the number of Pt on the surface increases. Interestingly, Pt₂/pr-TiO₂(110) system has the narrowest band gap of 0.05 eV among the other cases. This corresponds to a band gap narrowing of 1.22 eV relative to the Fermi energy of the pr-TiO₂(110). Although the band gap is underestimated by DFT due to improper description of the exchange-correlation energy, band gap narrowing must be absolute and so, experimentally verifiable. This value has been calculated to be 1.16 eV for the Pt₃ case.

In Pt₄ case, we examined initial adsorption structures including low energy gas phase rhombus and pyramid isomers on partially reduced surface. Relaxed cluster-surface combined system has been found to be the geometry as shown in Fig. 4c. Symmetrical rhombus form can be obtained by adding a Pt atom to Pt₃/pr-TiO₂ system in Fig. 4b. However, after relaxation, such a structure is energetically less favorable by 0.35 eV/cell. Comparably, Pt₄ in Fig. 4c, shows an increased coordination with O1's. This structure can also be obtained by adding a Pt to Pt₃/pr-TiO₂ so that Pt₄ lies between the two bridging oxygen rows. All these small Pt particles cluster around the vacancy site. Their geometries are different, in particular for Pt₄, from those on the stoichiometric surface, due to the surface charge distribution around the defect site. Pt particles oxidize and therefore bind to defective surface stronger than to the defect free one.

Pt₄ adsorption on the reduced surface induces thirteen flat-like occupied gap states due to the excess charge brought by the metal cluster, which is larger than that of the previous cases. Fermi energy occurs at just above the upmost lying flat state as seen in the top panel of Fig. 5. This corresponds to a narrowing of 1.06 eV relative to the band gap of the reduced surface. Since all Pt clusters bind so as to center around the defect site, all cases have contributions to the DOS's from these bonding Pt-Ti6c states that appear inside the VB with increasing Pt content. Indeed, Pt₄/pr-TiO₂(110) system has the largest partial DOS contribution inside the VB which essentially disperses similar to that of the Pt₃ case.

TABLE II. Calculated total binding energies (eV) of Pt clusters and corresponding average binding energies per Pt atom at TiO₂(110)-4×2 surfaces.

	stoichiometric	reduced ^a	reconstructed ^b
Pt	2.32 / 2.32	3.32 / 3.32	3.94 / 3.94
Pt ₂	1.74 / 0.87	2.22 / 1.11	4.20 / 2.10
Pt ₃	2.66 / 0.89	3.26 / 1.09	4.76 / 1.59
Pt ₄	2.98 / 0.75	3.38 / 0.85	4.54 / 1.14

^a with oxygen vacancy concentration $\theta=0.125$

^b added-row model of Onishi and Iwasawa⁴⁶

C. Pt_n on reconstructed rutile TiO₂(110) surface

The atomic resolution of the long range (1×2) phase of reconstructed rutile TiO₂(110) surface is difficult with experiments, numerous theoretical studies attempted to resolve the controversy regarding the surface morphology^{48–50}. Scanning tunneling microscopy (STM) and low-energy electron diffraction (LEED) experiments showed the existence of Ti₂O₃ added rows in agreement with the model proposed by Onishi and Iwasawa^{46,48,51–53}. We constructed this model of (1×2) surface by forming additional Ti₂O₃ rows along [001] at the top and the bottom facets of the relaxed stoichiometric slab with 7 trilayers. This turns out to be a symmetrical cell which prevents a fictitious dipole formation across the slab. We studied Pt cluster adsorption on 4×2 cell that accommodates separations of ~ 12 Å along [001] and ~ 13 Å along [010] to avoid any charge transfer between the periodic images of the metal adsorbates. The relaxed geometries of Pt_n/ar-TiO₂(110) systems are depicted in Fig. 6.

The electronic structure of added row model of the reconstructed surface was given by Kimura *et al.*²¹ and recently by Blanco-Rey *et al.*⁵². By employing pure DFT methods they obtained DOS peaks resulting from Ti₂O₃ row occupying the bottom of the CB. The origin of these DOS contributions are similar to Ti⁺³ states derived from oxygen vacancies on the reduced surface. Pure DFT is known to fail in describing these vacancy states predicting a metallic character.^{43–45} However, defect states appear 0.7–0.9 eV below the CB.^{36–39} Therefore, for (1×2) reconstruction, pure DFT must incorrectly predict Ti 3d states coming from the Ti₂O₃ row to appear inside, at the bottom of, the CB. We tried to obtain a reasonable electronic description of the added row model of reconstructed, bare and Pt_n ($n=1-4$) adsorbed surfaces by employing Dudarev *U* corrected spin polarized DFT calculations. Our tests showed that calculated band structure of TiO₂ is sensitive to relaxation of the atomic positions based on energy minimization of the computational cell. In this sense, supplementary *U* repulsion energy considerably changes the Ti–O bond lengths, resulting surface geometry, and so, the band structure.

Experimentally, Abad *et al.* observed the band gap state at 0.7 eV having Ti 3d character from the UPS He-I spectra for TiO₂(110)-(1×2)⁷⁵. In our calculations, the choice of $U = 4.5$ drives the Ti defect states from the CB edge down into the gap giving band gap of ~ 0.1 eV in the bottom panel of Fig. 7. Certainly, this value is underestimated due to the improper cancellation of the self interaction, a well known artifact of DFT. In addition to the appearance of defect states due to broken stoichiometry, reconstruction also changes the dispersion of states at the band edges. Our GGA+*U* calculations resulted in a ground state with spin multiplicity of 1.99 per (1×2) surface cell similar to the case of pr-TiO₂(110). Two satellite DOS peaks appear in the band gap associated with the excess charge on the Ti₂O₃ row. These defect

states strongly disperse over a width of ~ 1.3 eV in the gap and possess Ti $3d$ character. Fermi level occurs 2.16 eV above the VBM. If we compare band gap narrowing of 2.16 eV with experimental gap, we expect (1×2) phase of $\text{TiO}_2(110)$ to exhibit a photoemission at an energy consistent with the observation of Abad *et al.*⁷⁵

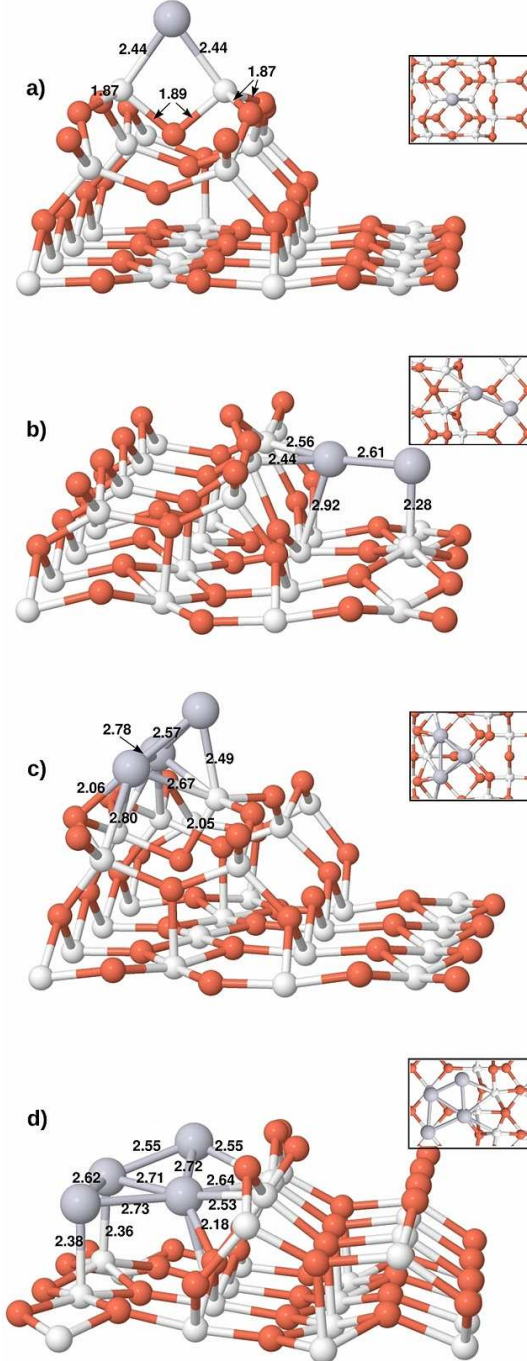


FIG. 6. (color online) Minimum energy structures of reconstructed rutile $\text{TiO}_2(110)$ surfaces with Pt_n ($n=1-4$) adsorbates. O, Ti, and Pt atoms are denoted by black (red), white small balls, and gray big balls, respectively. Bond lengths are shown in angstroms. The top view of the small Pt particles are presented in the insets are provided for visual convenience.

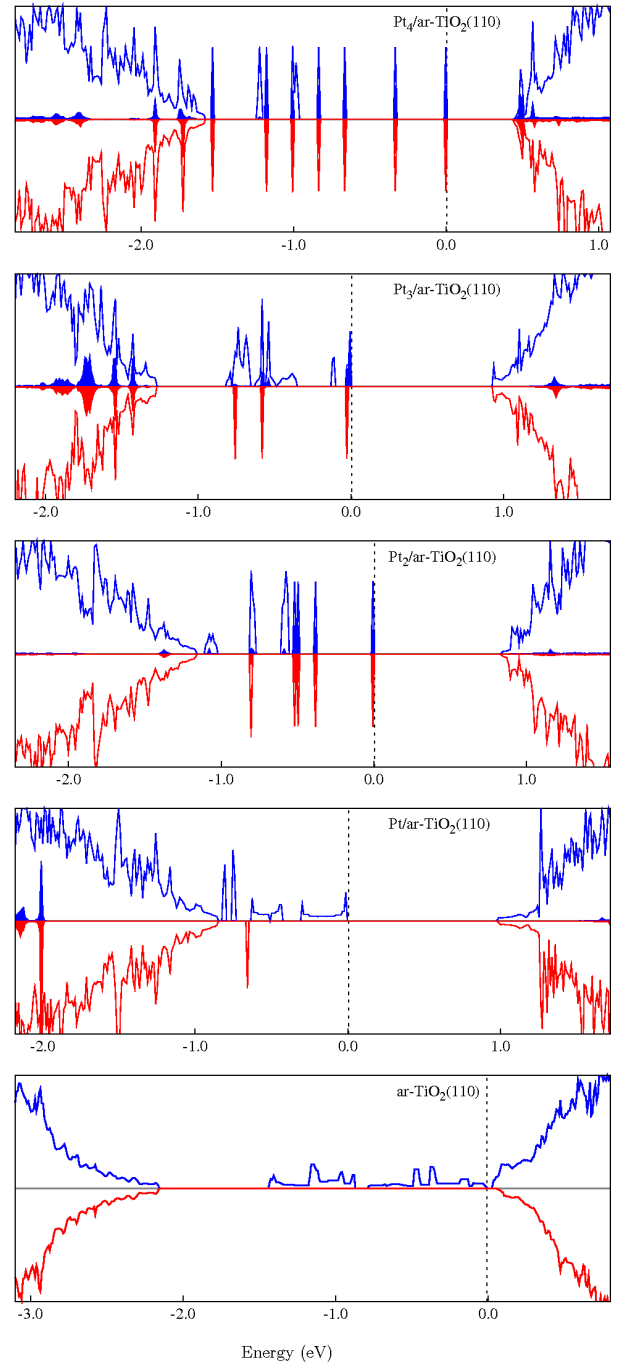


FIG. 7. (color online) Calculated projected and total DOS structures for Pt_n ($n=1-4$) on added row (ar) model of reconstructed rutile $\text{TiO}_2(110)$ - 4×2 surface for the low energy adsorption models shown in Fig. 6.

We considered various possible sites for Pt adsorption on the reconstructed (1×2) reduced surface. The minimum energy surface structure of single Pt adsorption is depicted in Fig. 6a. An isolated Pt atom gets adsorbed at the oxygen site over the terrace in between the two Ti cations lying along $[010]$ that are also labeled as $\text{Ti}(\text{iv})$ ⁴⁹. Pt pulls these Ti cations, and so, indirectly the oxygen underneath, forming a symmetrical tetrago-

nal group. The oxygen elevates up by 1.5 Å from its relaxed Ti_2O_3 row position. Pt–Ti equilateral bond length becomes 2.44 Å and Ti–O bonds are 1.89 Å belonging to the tetragon while the two Ti(iv)’s make four equidistant bonds with oxygens over the row reading 1.87 Å each. Pt on reconstructed surface has the strongest binding energy of 3.94 eV/atom among the other system considered in this study.

Electronically, adsorbate driven atomic dislocations on the $\text{TiO}_2(110)$ surface has a significant effect on its band structure. In particular, band edges are sensitive to any distortion on the Ti_2O_3 construction. For example, single Pt atom adsorption changes the valence and conduction band edges and offsets of the reconstructed rutile surface when we compare the corresponding DOS structures of ar- $\text{TiO}_2(110)$ systems with and without Pt atom in Fig. 7. For an isolated Pt, Fermi energy occurs at 0.85 eV above the VBM due to upper lying gap state. The band gap is widened by 0.92 eV in comparison to that of the clean reconstructed (1×2) surface. Single Pt atom on 4×2 cell corresponds to a low concentration coverage. It can only partially reoxidize the Ti(iv) defect states, which appear in the bottom panel of Fig. 7 for the majority-spin component. The states associated to these saturated dangling bonds as a result of Pt binding fall into the VB at around -2.0 eV. Remaining partially unsaturated defect states move down to lower energies leading to the gap widening. Their DOS exhibits two sharp van Hove singularities with dispersions weaker than those of the clean reconstructed surface. Non-bonding excess charge leads to one and two flat-like filled states just above the VBM for majority and minority spin components, respectively.

A Pt dimer energetically prefers to get adsorbed at the trench in interaction with two reactive Ti(iv) cations on the added row and with the in-plane Ti5c as shown in Fig. 6b. In comparison, the total energy of a 4×2 cell with Pt dimer over Ti5c row along [100] is interestingly just 0.04 eV higher than the lowest energy geometry. Evidently, Ti5c is an active site inside the trench. Other cases appear to be far less probable. For example, Pt_2 over and along the Ti_2O_3 row is energetically less favorable by 0.92 eV. In Fig. 6b, the dimer shows an extended length of 2.61 Å which is considerably larger than its isolated value of 2.33 Å, essentially due to strong Pt–Ti coupling. As a result of the Pt–Ti(iv) interactions having 2.44 and 2.56 Å bonds, the oxygen over the row changes its outward posture and shows an inward alignment. Moreover, Pt at Ti5c site pulls the Ti underneath out of its in-plane position by ~ 0.8 Å leading to a bond length of 2.28 Å. These dislocations distort the Ti_2O_3 group breaking its symmetry along [010].

Pt_2 particle brings six majority and five minority flat-like impurity states below the Fermi energy as shown in Fig. 7. In addition, a slightly more dispersing Pt driven state appear just above the VBM for the spin-up component. Fermi energy is determined by the upper lying impurity state at 1.17 eV above the VBM. Thus, the band gap is larger by 0.75 eV relative to that of ar- $\text{TiO}_2(110)$.

Evidently, the appearance of partial DOS contribution from mainly 5d electrons of the Pt cluster in the vicinity of the Fermi energy indicates that Pt_2 has non-bonding localized excess charge density which was absent in the case of an isolated Pt case.

We have investigated various probable adsorption structures for Pt_3 particle. Energetically, Pt trimer favors the on-the-row adsorption over an in-trench position as shown in Fig. 6c. Pt trimer forms in an equilateral triangle with a 2.78 Å and two 2.57 Å bonds. Pt_3 and Pt_1 cases have some common features. Topmost Pt atom pulls Ti(iv) atom so that the bond length becomes 2.49 Å similar to that of Pt/ar- $\text{TiO}_2(110)$. The sub-oxygen of the row that is denoted by its bond with Ti(iv) as 2.05 Å in Fig. 6c is pulled up as in the single Pt case. At the other side of the row Pt–Pt bond aligns with [100] pushing the two oxygens away so that, that side of the row bends outwards.

The DOS structure of Pt_3 /ar- $\text{TiO}_2(110)$ system displays some similarities with that of Pt_2 in that a number of impurity states appear below the Fermi energy exhibiting dominant Pt 5d character. Evidently, these weakly dispersing impurity states are brought by the excess charge density localized on the metal cluster. Similar to the case Pt_2 , Fermi level is determined by the upper lying flat-like state at 1.27 eV above the VBM that corresponds to a band gap widening of 0.90 eV with respect to bare reconstructed surface. On the other hand the offsets of the VB edges differ due to adsorbate induced different local surface relaxations. Pt_3 and a single Pt atom stick to the Ti_2O_3 group. Therefore the partial DOS contribution of bonding 5d electrons appear in the corresponding VBs. Since, the coordination number of Pt_3 with the added row is relatively larger compared to the Pt case, and since Pt_3 distorts the row more than a single Pt do, bonding Pt_3 – Ti_2O_3 states appear in the upper part of the VB.

The minimum energy structure for the Pt_4 case has been found to be as shown in Fig. 6d where the trench accommodates the cluster. We see that Pt_4 adsorption builds up on the Pt_2 /ar- TiO_2 skeleton by additional two platinum atoms so that a gas phase Pt_4 forms in the trench. Inward position of the row oxygen closer to the cluster is similar to that of the Pt_2 case. Two adjacent vertical Pt–Ti5c bonds become 2.38 and 2.36 Å that are slightly larger than the value of 2.28 Å for the Pt dimer on the surface. They reduce the interaction strength by relatively better saturating the dangling bonds. Clearly, off-planar form of the rhombus gets distorted due to Pt–Ti(iv) interactions so that the side bonds are considerably extended. As in the case of Pt_2 adsorption the added row construction gets pulled towards Pt_4 through Pt–Ti(iv) interaction. Similar arguments can be made for Pt_3 and Pt–surface cases.

In the top panel of Fig. 7, the CB edge is determined by empty Pt_4 6s states. Eight and seven flat-like occupied impurity states appear in the DOS for the spin up and down components, respectively, associated mainly with

the $5d$ electrons of Pt_4 cluster. The flat impurity state lying 1.59 eV above the VBM sets the Fermi level corresponding to a band gap larger by 0.28 eV relative to that of the bare reconstructed surface. The positioning of the cluster–surface bonding states inside the VB is similar to Pt_2 case which shows common adsorption characteristics.

Pt adsorbates prefer to bind to Ti atoms on the added-row model of the reconstructed surface since Ti_2O_3 stoichiometry leads to oxygen deficiency. Hence, oxygens on the added-row become less reactive compared to Ti cations. As a trend, odd and even numbered cluster sizes show different adsorption characteristics. While clusters with odd number of Pt atoms energetically prefer to be on the added row terrace, even numbered ones relax into the trench at one side of the row. Furthermore, it is interesting to see that Pt_4 –surface system has common elements with Pt_2 case as a building block, although they were considered distinctly and their initial structures were not relevant in this sense. Pt clusters in the trench breaks the symmetrical formation of the added row construction along $[010]$ while on-the-row adsorption more or less resumes the symmetry.

IV. CONCLUSIONS

A systematic analysis of atomic and electronic structure of small Pt particles, from monomers to tetramers, supported on regular and defect sites of $\text{TiO}_2(110)$ surface has been presented based on Hubbard U corrected hybrid DFT calculations using Dudarev’s approach. The atomic structure of the titania supported Pt clusters determined by the surface stoichiometry that constrains the charge density. The calculated binding energies of Pt particles on the Onishi and Iwasawa model of the (1×2) surface happens to be greater than those of the corresponding adsorption systems on partially reduced (oxygen vacant) and stoichiometric surfaces due to electron delocalization from the reduced Ti sites. Interestingly, these chemisorbed Pt clusters form geometries similar to their gas phase structures except Pt_4 at the defect site on the partially reduced surface where bridging O–Pt interaction plays a role. In fact, binding energies per Pt atom

decreases as the Pt cluster size increases due to stronger meta-metal coordination. Thus, large Pt particles show 3D-like nucleation.

We demonstrated that DFT+U method reproduces experimentally observed gap states for the non-stoichiometric surfaces where electronic correlation is of vital importance. In particular, Ti(iv) $3d$ states have been shown to fall within the band gap of $\text{TiO}_2(110)-(1\times 2)$ reconstructed surface. Those were incorrectly predicted by pure DFT to be inside the CB giving a metallic character, similar to oxygen vacancy states. Interaction of small Pt clusters with the $\text{TiO}_2(110)$ delocalizes charge causing distortion in the geometry around the adsorption site. This significantly alters the band edges of the titania support and also brings band-gap states depending on the cluster size. The position of these defect states show strong dependence on the lattice relaxations. Consequently, adsorbate–substrate coupling leads to significant band gap narrowing for bulk terminated and partially reduced surfaces while it gives rise to a gap widening in the case of reconstructed surface. No metallization occurs for Pt_n/TiO_2 ($n = 1-4$) systems. These results provide good insight into the effect of deposition of small Pt particles on the atomic and electronic structure of $\text{TiO}_2(110)$ surfaces with adsorbates. The detailed analysis of the differences in DOS upon Pt cluster adsorption puts forward a sound physical picture for adsorbate-substrate interface properties. In $\text{Pt}_n\text{--TiO}_2(110)$ chemisorption systems, the appearance of well localized non-bonding Pt impurity states might be useful for catalytic and photovoltaic applications.

ACKNOWLEDGMENTS

We acknowledge partial financial support from TÜBİTAK, The Scientific and Technological Research Council of Turkey (Grant no: TBAG 107T560). In conjunction with this project, computational resources were provided by ULAKBİM, Turkish Academic Network & Information Center. VÇ and EM also acknowledge secondary support from Balıkesir University through BAP project number 2010/37.

* Corresponding author email : emete@balikesir.edu.tr; Also at Institute of Theoretical and Applied Physics (ITAP) Turunç, Muğla, Turkey

¹ V. E. Henrich and P. A. Cox, *The Surface Science of Metal Oxides*, (Cambridge Univ. Press, Cambridge, 1994).

² A. Fujishima and K. Honda, *Nature (London)* **238**, 37 (1972).

³ U. Diebold, *Surf. Sci. Rep.* **48**, 53 (2003).

⁴ A. Hangfeldt and M. Grätzel, *Chem. Rev.* **95**, 49 (1995).

⁵ M. Grätzel, *Nature (London)* **414**, 338 (2001).

⁶ S. Khan, J. M. Al-Shahry, and W. B. Ingler, *Science* **297**, 2243 (2002).

⁷ M. Chen, Y. Cai, Z. Yan, and D. W. Goodman, *J. Am. Chem. Soc.* **128**, 6341 (2006).

⁸ P. Finetti, F. Sedona, G. A. Rizzi, U. Mick, F. Sutara, M. Svec, V. Matolin, K. Schierbaum, and G. Granozzi, *J. Phys. Chem. C* **111**, 869 (2007).

⁹ J. M. Wu and C. J. Chen, *J. Am. Ceram. Soc.* **73**, 420 (1990).

¹⁰ G. L. Griffin and K. L. Sieferring, *J. Electrochem. Soc.* **137**, 1206 (1990).

¹¹ A. K. See, M. Thayer, and R. A. Bartynski, *Phys. Rev. B* **41**, 13722 (1993).

¹² Z. Zhang, S.-P. Jeng, and V. E. Henrich, *Phys. Rev. B* **43**,

- 12004 (1991).
- ¹³ D. Novak, E. Garfunkel, and T. Gustafsson, *Phys. Rev. B* **50**, 5000 (1994).
 - ¹⁴ U. Diebold, J. F. Anderson, K. O. Na, and D. Vanderbilt, *Phys. Rev. Lett.* **77**, 1322 (1996).
 - ¹⁵ G. Charlton, P. B. Hoowes, C. L. Nicklin, P. Steadman, J. S. G. Taylor, C. A. Muryn, S. P. Harte, J. Mercer, R. McGrath, D. Norman, T. S. Turner, and G. Thornton, *Phys. Rev. Lett.* **78**, 495 (1997).
 - ¹⁶ E. Asari, T. Suzuki, H. Kawanowa, J. Ahn, W. Hayami, T. Aizawa, and R. Souda, *Phys. Rev. B* **61**, 5679 (2000).
 - ¹⁷ R. Lindsay, A. Wander, A. Ernst, B. Montanari, G. Thornton, and N. M. Harrison, *Phys. Rev. Lett.* **94**, 246102 (2005).
 - ¹⁸ M. Ramamoorthy, R. D. King-Smith, and D. Vanderbilt, *Phys. Rev. B* **49**, 7709 (1994).
 - ¹⁹ M. Ramamoorthy, D. Vanderbilt, and R. D. King-Smith, *Phys. Rev. B* **49**, 16721 (1994).
 - ²⁰ P. J. D. Lindan, N. M. Harrison, M. J. Gillan, and J. A. White, *Phys. Rev. B* **55**, 15919 (1997).
 - ²¹ S. Kimura and M. Tsukada, *Appl. Surf. Sci.* **130–132**, 587 (1998).
 - ²² N. M. Harrison, X. G. Wang, J. Muscat, and M. Scheffler, *Faraday Discuss.* **114**, 305 (1999).
 - ²³ D. Vogtenhuber, R. Podlucky, A. Neckel, S. G. Steinemann, and A. J. Freeman, *Phys. Rev. B* **49**, 2099 (1994).
 - ²⁴ P. Reinhardt and B. A. Heß, *Phys. Rev. B* **50**, 12015 (1994).
 - ²⁵ S. P. Bates, G. Kresse, and M. J. Gillan, *Surf. Sci.* **385**, 386 (1997).
 - ²⁶ R. A. Evarestov and A. V. Bandura, *Int. J. Quantum Chem.* **96**, 282 (2004).
 - ²⁷ A. V. Bandura, D. G. Sykes, V. Shapovalov, T. N. Troung, J. D. Kubicki, and R. A. Evarestov, *J. Phys. Chem. B* **108**, 7844 (2004).
 - ²⁸ T. Bredow, L. Giordano, F. Cinquini, and G. Pacchioni, *Phys. Rev. B* **70**, 035419 (2004).
 - ²⁹ H. Sano, G. Mizutani, W. Wolf, and R. Podlucky, *Phys. Rev. B* **70**, 125411, (2004).
 - ³⁰ Y.-F. Zhang, W. Lin, Y. Li, K.-I. Ding, and J.-Q. Li, *J. Phys. Chem. B* **109**, 19270 (2005).
 - ³¹ A. Kiejna, T. Pabisiak, and S. W. Gao, *J. Phys.: Condens. Matter* **18**, 4207 (2006).
 - ³² S. J. Thompson and S. P. Lewis, *Phys. Rev. B* **73**, 073403 (2006).
 - ³³ K. J. Hameeuw, G. Cantele, D. Ninno, F. Trani, and G. Iadonisi, *J. Chem. Phys.* **124**, 024708 (2006).
 - ³⁴ P. M. Kowalski, B. Meyer, and D. Marx, *Phys. Rev. B* **79**, 115410 (2009).
 - ³⁵ F. Labat, P. Baranek, and C. Adamo, *J. Chem. Theory Comput.* **4**, 341 (2008).
 - ³⁶ V. E. Henrich, G. Dresselhaus, and H. J. Zeiger, *Phys. Rev. Lett.* **36**, 1335 (1976).
 - ³⁷ W. Göpel, J. A. Anderson, D. Frankel, M. Jaehrig, K. Phillips, J. A. Schäfer, and G. Rocker, *Surf. Sci.* **139**, 333 (1984).
 - ³⁸ R. L. Kurtz, R. Stockbauer, T. E. Madey, E. Román, and J. L. De Segovia, *Surf. Sci.* **218**, 178 (1989).
 - ³⁹ M. A. Henderson, *Surf. Sci.* **400**, 203 (1998).
 - ⁴⁰ S. Wendt, P. T. Sprunger, E. Lira, G. K. H. Madsen, Z. Li, J. O. Hansen, J. Matthiesen, A. Blekinge-Rasmussen, E. Lægsgaard, B. Hammer, and F. Besenbacher, *Science* **320**, 1755 (2008).
 - ⁴¹ P. Kruger, S. Bourgeois, B. Domenichini, H. Magnan, D. Chandesris, P. Le Fevre, A. M. Flank, J. Jupille, L. Floreno, A. Cossaro, A. Verdini, and A. Morgante, *Phys. Rev. Lett.* **100**, 055501 (2008).
 - ⁴² Greg A. Kimmel and Nikolay G. Petrik, *Phys. Rev. Lett.* **100**, 196100 (2008).
 - ⁴³ B. J. Morgan and G. W. Watson, *Surf. Sci.* **601**, 5034 (2007).
 - ⁴⁴ C. J. Calzado, N. C. Hernandez, and J. F. Sanz, *Phys. Rev. B* **77**, 045118 (2008).
 - ⁴⁵ M. Nolan, S. D. Elliot, J. S. Mulley, R. A. Bennett, M. Basham, and P. Mulheran, *Phys. Rev. B* **77**, 235424 (2008).
 - ⁴⁶ H. Onishi and Y. Iwasawa, *Surf. Sci. Lett.* **313**, 783 (1994).
 - ⁴⁷ Q. Guo, I. Cocks, and E. M. Williams, *Phys. Rev. Lett.* **77**, 3851 (1996).
 - ⁴⁸ C. L. Pang, S. A. Haycock, H. Raza, P. W. Murray, G. Thornton, O. Gülseren, R. James, and D. W. Bullett, *Phys. Rev. B* **58**, 1586 (1998).
 - ⁴⁹ S. D. Elliott and S. P. Bates, *Phys. Rev. B* **65**, 245415 (2002).
 - ⁵⁰ S. D. Elliott and S. P. Bates, *Phys. Rev. B* **67**, 035421 (2003).
 - ⁵¹ K. F. McCarty and N. C. Bartelt, *Phys. Rev. Lett.* **90**, 046104 (2003).
 - ⁵² M. Blanco-Rey, J. Abad, J. Méndez, M. F. López, J. A. Martín-Gago, and P. L. de Andrés, *Phys. Rev. Lett.* **96**, 055502 (2006).
 - ⁵³ M. Blanco-Rey, J. Abad, C. Rogero, J. Méndez, M. F. López, E. Román, J. A. Martín-Gago, and P. L. de Andrés, *Phys. Rev. B* **75**, 081402(R) (2007).
 - ⁵⁴ K. T. Park, M. Pan, V. Meunier, and E. W. Plummer, *Phys. Rev. B* **75**, 245415 (2007).
 - ⁵⁵ N. Shibata, A. Goto, S.-Y. Choi, T. Mizoguchi, S. D. Findlay, T. Yamamoto, and Y. Ikuhara, *Science* **322**, 570 (2008).
 - ⁵⁶ Y. Gai, J. Li, S.-S. Li, J.-B. Xia, and S.-H. Wei, *Phys. Rev. Lett.* **102**, 036402 (2009).
 - ⁵⁷ A. L. Linsebigler, G. Q. Lu, and J. T. Yates, *Chem. Rev.* **95**, 735 (1995).
 - ⁵⁸ H. Iddir, S. Ögüt, N. D. Browning, and M. M. Disko, *Phys. Rev. B* **72**, 081407(R) (2005); *Phys. Rev. B* **73**, 039902(E) (2006).
 - ⁵⁹ D. Pillay and G. S. Hwang, *J. Mol. Struct.:THEOCHEM* **771**, 129 (2006).
 - ⁶⁰ X.-Q. Gong, A. Selloni, O. Dulub, P. Jacobson, and U. Diebold, *J. Am. Chem. Soc.* **130**, 130 (2008).
 - ⁶¹ G. Kresse and J. Hafner, *Phys. Rev. B*, **47**, 558 (1993).
 - ⁶² J. P. Perdew, K. Burke, and M. Ernzerhof, *Phys. Rev. Lett.* **77**, 3865 (1996).
 - ⁶³ P. E. Blöchl, *Phys. Rev. B* **50**, 17953 (1994).
 - ⁶⁴ G. Kresse and D. Joubert, *Phys. Rev. B* **59**, 1758 (1999).
 - ⁶⁵ S. L. Dudarev, G. A. Botton, S. Y. Savrasov, C. J. Humphreys, and A. P. Sutton, *Phys. Rev. B* **57**, 1505 (1998).
 - ⁶⁶ H. Monkhorst and J. Pack, *Phys. Rev. B* **13**, 5188 (1976).
 - ⁶⁷ M. N. Huda, M. K. Niranjana, B. R. Sahu, and L. Kleinman, *Phys. Rev. A* **73**, 053201 (2006).
 - ⁶⁸ M. B. Airola and M. D. Morse, *J. Chem. Phys.* **116**, 1313 (2002).
 - ⁶⁹ S. Taylor, G. W. Lemire, Y. M. Hamrick, Z. Fu, and M. D. Morse, *J. Chem. Phys.* **89**, 5517 (1988).
 - ⁷⁰ A. Grushow and K. M. Ervin, *J. Chem. Phys.* **106**, 9580 (1997).

- ⁷¹ Li Xiao and Lichang Wang, J. Phys. Chem. A **108**, 8605 (2004).
- ⁷² A. R. Miedema, Z. Metallkd. **69**, 287 (1978).
- ⁷³ S. H. Yang, D. A. Drabold, J. B. Adams, P. Ordejon, and K. Glassford, J. Phys.: Condens. Matter **9**, L39 (1997).
- ⁷⁴ H. R. Sadeghi and V. E. Henrich, J. Catal. **109**, 1 (1988).
- ⁷⁵ J. Abad, C. Rogero, J. Mendez, M. F. Lopez, J. A. Martin-Gago, and E. Román, Appl. Surf. Sci. **234**, 497 (2004).